Logarithmic Time Course of Sensory Adaptation in Electrosensory Afferent Nerve Fibers in a Weakly Electric Fish

ZHIAN XU, JEREMY R. PAYNE, AND MARK E. NELSON
Department of Molecular and Integrative Physiology and The Beckman Institute, University of Illinois at
Urbana-Champaign, Urbana, Illinois 61801

SUMMARY AND CONCLUSIONS

1. We recorded single unit activity from individual primary electrosensory afferent axons in the posterior branch of the anterior lateral line nerve of gymnotid weakly electric fish, *Apteronotus leptorhynchus*. We analyzed the responses of P-type (probability-coding) afferent fibers to externally applied amplitude step changes in the quasi-sinusoidal transdermal potential established by the fish's own electric organ discharge (EOD).

2. In response to AM step increases in transdermal potential, the firing rate of P-type afferents exhibited an abrupt increase followed by an initially rapid and subsequently more gradual decay back toward the baseline level. Afferent responses continued to adapt slowly throughout the duration of prolonged step stimuli lasting >100 s. The time course of sensory adaptation was similar for all units tested.

3. We introduce a new functional form for describing the time course of sensory adaptation in which the change in firing rate Δr decays logarithmically with time: $\Delta r(t) = A/[B \ln (t) + 1]$. This logarithmic form accurately describes the adaptation time course of P-type afferents over five decades in time, from milliseconds to hundreds of seconds, with only two free parameters. Using a nonlinear least-squares fitting technique, we obtained a mean value of the parameter B, which characterizes the adaptation time course, of 0.149 ± 0.028 (mean $\pm$ SD, $n = 49$).

4. We compare logarithmic fits with traditional multiexponential and power law forms and demonstrate that the logarithmic form yields a better characterization of P-type afferent responses. This analysis helps explain the variability in previously reported adaptation time constants, which have ranged from 0.2 to 3.4 s, in gymnotid P-type afferents.

5. We tested the linearity of P-type afferent responses using positive and negative AM steps of varying amplitudes. Aside from nonlinearities associated with rectification (firing rates cannot be negative) and saturation (firing rates cannot exceed the EOD frequency), we found that P-type afferent responses scaled linearly with stimulus amplitude.

6. Based on the observed linearity, we predict the frequency domain response characteristics of P-type afferents and find that the predicted gain and phase are in good agreement with experimental measurements using sinusoidal AM stimuli over a range of AM frequencies from 1 to 100 Hz. Thus the logarithmic parameterization of the step response appears to accurately capture the response dynamics of P-type afferents over a wide range of behaviorally relevant AM frequencies.

7. We conclude that the temporal filtering properties of pyramidal cells in the medullary electrosensory nucleus, the electrosensory lateral line lobe (ELL), need to be reevaluated in light of the logarithmic adaptation time course in the periphery, and we discuss implications for the role of P-type afferents in driving a feedback gain control mechanism that regulates ELL pyramidal cell responsiveness.

INTRODUCTION

The electrosensory system of gymnotiform weakly electric fish has become an important model system for studies of neural computation and adaptive sensory processing (reviews: Bastian 1994; Heiligenberg 1991; Nelson 1994b). These freshwater fish from Central and South America generate weak electric fields around their bodies by means of specialized electric organs in the tail. In the species *Apteronotus leptorhynchus* (brown ghost knife fish) the electric organ is derived from spinal axons and discharges at a constant rate ranging from 600 to 1,200 Hz depending on the individual fish. Each cycle of the quasi-sinusoidal electric organ discharge (EOD) generates a dipole-like electric field distribution around the fish (Knudsen 1975), with potentials near the fish that are typically a few millivolts in amplitude with respect to a remote reference (Rasnow et al. 1993). Perturbations in the electric field due to nearby objects, or the interference of electric fields from other weakly electric fish, give rise to local changes in the sinusoidally varying potential across the skin (transdermal potential) that is established by the fish's own EOD. The resulting amplitude and phase modulations are detected by specialized electroreceptor organs distributed over most of the body surface of the fish; these organs provide the animal with information that is used in communication, navigation, and electrolocation (review: Bullock and Heiligenberg 1986).

The first stage of information processing in the electrosensory system involves the encoding of changes in local transdermal potential into trains of action potentials in primary afferent nerve fibers. Changes in transdermal potential are detected by two anatomically distinct classes of electroreceptor organs in the skin: ampullary organs respond to low-frequency (DC–20 Hz) electric fields of extrinsic origin, whereas tuberous organs are specialized for detecting amplitude and phase modulations of signals near the carrier frequency of the EOD (review: Zakon 1986). Certain gymnotiforms, such as *Apteronotus,* have a continuous, quasi-sinusoidal (wave-type) EOD, whereas others have an intermittent (pulse-type) discharge. For species with wave-type EODs, tuberous receptor organs can be classified as T type (time coder) or P type (probability coder) based upon the firing characteristics of the primary afferent nerve fiber that innervates them. T- and P-type afferents fire at most one spike per EOD cycle with spike times phase-locked to the EOD cycle, but the phase-locking is much tighter in T units. T units fire regularly on every EOD cycle, whereas P units fire irregularly with a per-cycle firing probability that

depends upon stimulus intensity. T-type afferents primarily encode information about stimulus phase as changes in spike timing, whereas P-type afferents primarily encode information about stimulus amplitude as changes in firing probability (Scheich et al. 1973). These two physiologically defined categories appear to correspond to anatomically distinct classes of tuberous receptor organs (Zakon 1993). In *Apteronotus*, almost all of the tuberous receptor organs in the trunk region are of the P type (Hagiwara et al. 1965; Szabo 1974).

In response to an amplitude-modulated (AM) step increase in local transdermal potential, P-type afferents exhibit an abrupt increase in per-cycle firing probability; this increase subsequently adapts back toward the baseline level. Although the species *A. leptorhynchus* has become widely used for studies of central electrosensory processing in weakly electric fish, there are currently no published results on the time course of sensory adaptation in primary electrosensory afferents in this species. In a closely related species, *A. albifrons*, which has a similar EOD frequency range, Hagiwara et al. (1965) reported adaptation time constants ranging from 0.7 to 2.0 s and Hopkins (1976) reported a range from less than 0.5 to more than 2.0 s. Hopkins also noted that adaptation time constants appeared to be highly variable for individual afferent fibers and appeared to depend upon the stimulus conditions. In another wave-type gymnotid, *Eigenmannia virescens*, which has a lower EOD frequency range (300–400 Hz), Hopkins (1976) reported a similar range of time constants (between 0.2 and 3.4 s) and again noted that the determinants of adaptation time course were complex. Scheich et al. (1973) reported that the adaptation time course for P-type afferents in *Eigenmannia* had an average time constant of ~3 s but noted that the time course was not well described by a single exponential and that the initial adaptation could be much faster. A study by Shumway and Maler (1989) reported time constants of $\tau_{\text{fast}} = 0.875 \pm 0.496$ s and $\tau_{\text{slow}} = 1.785 \pm 0.274$ s (means $\pm$ SD) for biexponential fits to the afferent adaptation time course in *Eigenmannia*. In all of these studies, P-type afferent responses were described as partially adapting (phasic-tonic) in nature.

Our objectives in undertaking this study were twofold. First, we wished to characterize the time course of sensory adaptation in P-type afferents in *A. leptorhynchus*, because this species has become widely used for studies of central electrosensory processing, including those in our own laboratory. Second, we hoped that this study could help clarify the nature and source of the variability in previously reported adaptation time constants for P-type afferents in closely related gymnotid species, which span more than an order of magnitude (from 0.2 to 3.4 s). In general, studying the response dynamics of sensory neurons is important because it yields insights into temporal information processing mechanisms in the nervous system and provides clues about the sorts of signals in the environment that are of functional relevance to the animal. In the electrosensory system in particular, an accurate characterization of afferent response dynamics is crucial for neural modeling studies of gain control and adaptive filtering in the electrosensory lateral line lobe (ELL), a medullary sensory nucleus (Nelson 1993, 1994a; Payne et al. 1994), because the descending signals that con-

trol the gain and spatiotemporal filtering properties of ELL neurons are thought to be driven indirectly by P-type primary afferent inputs (Bastian 1986a,b; Bastian and Bratton 1990; Bastian and Courtright 1991).

METHODS

A total of 11 male and female adult (12–17 cm long) weakly electric fish of the species *A. leptorhynchus* (brown ghost knife fish) were used in this study. Fish were housed in laboratory aquaria and maintained on a 12 h light:12 h dark cycle. Water conditions in the holding tanks were maintained at a temperature of 27–28°C, pH of 6.5–6.9, and conductivity of 200–300 μmho/cm. Experiments were carried out in the middle of a rectangular Plexiglas tank (41 × 41 × 15 cm³) with water conditions adjusted to match the temperature, pH and conductivity of the home tanks.

Surgical procedure

Fish were anesthetized lightly by immersion in 100 ppm tricaine methanesulfonate (MS-222, Sigma) for 2 min, then immobilized with an intramuscular injection of 3 μl 10% gallamine triethiodide (Flaxedil, Sigma) and subsequently respirated with a constant flow of fresh aerated water provided through a mouth tube. The EOD from the neurogenic electric organ remained intact following the Flaxedil injection. Fish were held gently against a foam pad on a Plexiglas stand in the middle of the experimental tank with the dorsal surface of the head slightly higher that the rest of the body, such that the site of surgical exposure was just above the water level and most of the electroreceptors on the trunk of the fish were submerged. The posterior branch of the left anterior lateral line nerve (pALLN), which innervates trunk electroreceptors, was exposed ~1 mm rostral to the insertion of the pectoral fin, immediately dorsal to the lateral line. Lidocaine hydrochloride (2%) was applied locally to the skin before nerve exposure. The exposed nerve was bathed periodically in Ringer's solution (Bastian 1974) throughout the experiment. All surgical procedures were reviewed and approved by the Laboratory Animal Care and Advisory Committee at the University of Illinois at Urbana-Champaign.

Nerve recording

Action potentials from individual pALLN afferents were recorded with sharp glass micropipettes (impedance 10–30 MΩ) filled with 3 M KCl solution. The recording electrode was positioned in the intact nerve using a piezoelectric microdrive (Burleigh 7010). Nerve activity was recorded differentially with a unity-gain DC preamplifier (A-M Systems 1600), amplified by an AC amplifier (A-M Systems 1700) with a gain of 1,000, and bandpass filtered between 10 Hz and 5 kHz (40 dB/decade rolloff). A reference signal for the differential recording was provided by a fine silver wire electrode positioned in the exposure site near the nerve, so as to minimize the artifact from the fish's EOD.

The pALLN carries afferent fibers from both ampullary and tuberous electroreceptors; only P-type tuberous afferents were recorded in these experiments. Tuberous afferents were identified by applying a 5 Hz sinusoidal AM "search stimulus" to the experimental bath (see below) to preferentially excite tuberous receptors. Ampullary receptors did not respond to this AM search stimulus. A few T-type tuberous afferents, which are identified easily by their regular firing pattern at the EOD frequency, were encountered over the course of these experiments but were not studied. The vast majority of tuberous afferents in the pALLN are P type and can be identified readily by an irregular baseline firing pattern, which can be modulated by the search stimulus. No attempt was made in this study to determine the precise location of the electroreceptor organ corresponding to each P-type afferent fiber. A total of

117 P-type afferents were analyzed in this study with the following distribution: analysis of baseline activity, 117; single-trial long-duration step responses, 49; multi-trial short-duration step responses, 23; analysis of response linearity (full amplitude-series), 10; long-duration baseline controls, 26.

Stimulation and calibration

Stimuli consisted of AM step changes in the quasi-sinusoidal transdermal potential established by the fish's own EOD. AM waveform envelopes were generated with a programmable arbitrary function generator (Wavetek model 95), scaled to the desired intensity with a programmable attenuator (Weinschell model 3210), multiplied with the EOD carrier signal using an analog multiplier (Tucker-Davis), and delivered to the experimental tank through an optical stimulus isolator (A-M Systems 2200) via two 1.3-cm diam, 31-cm long carbon rods. The stimulus rods were placed horizontally, just under the surface of the water on either side of the fish, 17 cm from the midline, and parallel to the rostral-caudal axis. In this orientation, current flowing between the stimulus rods was perpendicular to the fish's lateral body surfaces. The fish's EOD signal was recorded from a pair of vertical carbon electrodes placed near the head and tail of the fish. The AM stimulus intensity was calibrated with respect to the transdermal potential change measured between an intramuscular reference electrode placed in the fish's back and a recording electrode outside the skin on the lateral trunk of the fish. Baseline (unstimulated) transdermal potentials had a root mean square (rms) value ranging from 0.4 to 1.5 mV (rms). A 0 dB stimulus (the maximum intensity used in this experiment) was defined as one that produced a 1 mV (rms) increase in transdermal potential. Stimulus intensities ranged from -25 to 0 dB. Typically, we were able to maintain stable recordings from pALLN fibers for periods of a few hundred seconds; thus long-duration step stimuli (duration $\geq$ 100 s) were presented as single trials, whereas short-duration step stimuli (duration $\leq$ 1 s) were presented as sets of 20–100 trials.

Data collection and analysis

All signals (nerve recording, EOD, transdermal potential, modulation waveform) were sampled digitally at 17 kHz with custom data acquisition software running on a Sun workstation (SPARC-station 2) equipped with a multifunction data acquisition card (Analyx Systems ADDA1418-166) and stored on magnetic disk for further processing. All data analysis procedures were carried out on Sun workstations using both custom software and a commercially available software package MATLAB (The MathWorks). Spike events in the nerve recording were identified by a threshold criterion and time-stamped with a resolution of 60 μs. Estimates of instantaneous firing rates used either linearly or logarithmically spaced bin edges. For multi-trial data records, firing rate estimates for each bin were computed by averaging the number of spike events across trials, and dividing by the bin width. For single-trial data records, rate estimates were computed from the number of interspike intervals wholly contained within the bin plus the fractional intervals associated with the first and last spike divided by the bin width. Fractional intervals are defined as the ratio of the time interval from the first or last spike in the bin to the bin edge, divided by the time interval to the nearest spike that falls outside the bin. The difference between the two rate estimation methods was found to be significant only when a bin contains just a few spikes, in which case the latter procedure provides lower statistical variability at the cost of a slight temporal smoothing of the response between adjacent bins.

The adaptation time course was parameterized using the following functional forms to describe the change in firing rate in response to AM step stimuli: 1) logarithmic: $\Delta r(t) = A/[B \ln (t) + 1]$;

2) multiexponential: $\Delta r(t) = A_1 e^{-t/\tau_1} + A_2 e^{-t/\tau_2} + \cdots + A_n e^{-t/\tau_n} + C$; 3) power law: $\Delta r(t) = At^{-k}$; and 4) "informational": $\Delta r(t) = A \ln (1 + \lambda/t)$ where $\Delta r(t)$ is the change in afferent firing rate in impulses per second above baseline and t is time relative to stimulus onset. Form 4 is labeled "informational" because it was developed by Norwich and McConville (1991) using concepts from information theory (see DISCUSSION). To fit each of these functional forms to the observed response data, the appropriate parameters (A_i, B, τ_i, k, λ) were varied in a least squares fitting procedure to minimize the χ^2 between the predicted and observed rate change. The χ^2 minimization was carried out using a constrained nonlinear optimization routine provided by the MATLAB Optimization Toolbox. The goodness-of-fit was evaluated based on the observed χ^2 per degrees-of-freedom (χ^2/ν), where the number of degrees-of-freedom (ν) is equal to the number of data bins in the fit minus the number of free parameters.

Frequency domain analysis

To compute the frequency domain response characteristics from the logarithmic parameterization of the step response, we first took the temporal derivative of the first equation to obtain the impulse response, and then evaluated numerically the impulse response function at discrete time values ranging from 0.002 to $\sim$1,000 s in 0.002-s steps. These time values were selected to span the time scales of interest for P-type afferent adaptation, while avoiding the singularity at short time scales (see DISCUSSION) and including the slowly decaying tail of the response at long time scales. Using a total of 2^{19} points in the time domain, we computed the discrete Fourier transform using a radix-2 fast Fourier transform algorithm provided as a built-in MATLAB function.

RESULTS

Baseline activity

Baseline activity was analyzed in 117 P-type afferent fibers (11 fish) in the absence of any externally imposed stimulus, but in the presence of the EOD. We refer to afferent activity under these conditions as baseline, rather than spontaneous, to reflect the continuous presence of the carrier signal due to the fish's own EOD. The baseline condition is the functionally relevant case for wave-type weakly electric fish, because the EOD signal is present continuously under natural conditions in these animals. The EOD frequency (f_{EOD}) ranged from 638 to 982 Hz in the 11 fish tested (open bars in Fig. 1A). The baseline firing rate (r_{base}) of P-type afferents ranged from 70 to 571 spikes/s with a mean of 261 $\pm$ 98 spikes/s ($n = 117$). The distribution of baseline firing rates is shown in Fig. 1A (solid bars). P-type afferents fire at most one spike per EOD cycle, thus the average probability (P) of generating a spike per EOD cycle is obtained by dividing the baseline firing rate by the EOD frequency ($P = r_{base}/f_{EOD}$). Under baseline conditions, P ranged from 0.10 to 0.60 with a mean of 0.33 $\pm$ 0.13 ($n = 117$) as shown in Fig. 1B. When multiplied by the EOD frequency of an individual fish, the distribution in Fig. 1B can be used to estimate the distribution of baseline firing rates for P-type afferents in a single fish.

Bursty versus nonbursty afferents

Bastian (1981a) has reported previously that P-type afferents in *Apteronotus* appear to fall into bursty and nonbursty categories. Bursty units tend to produce clusters of action
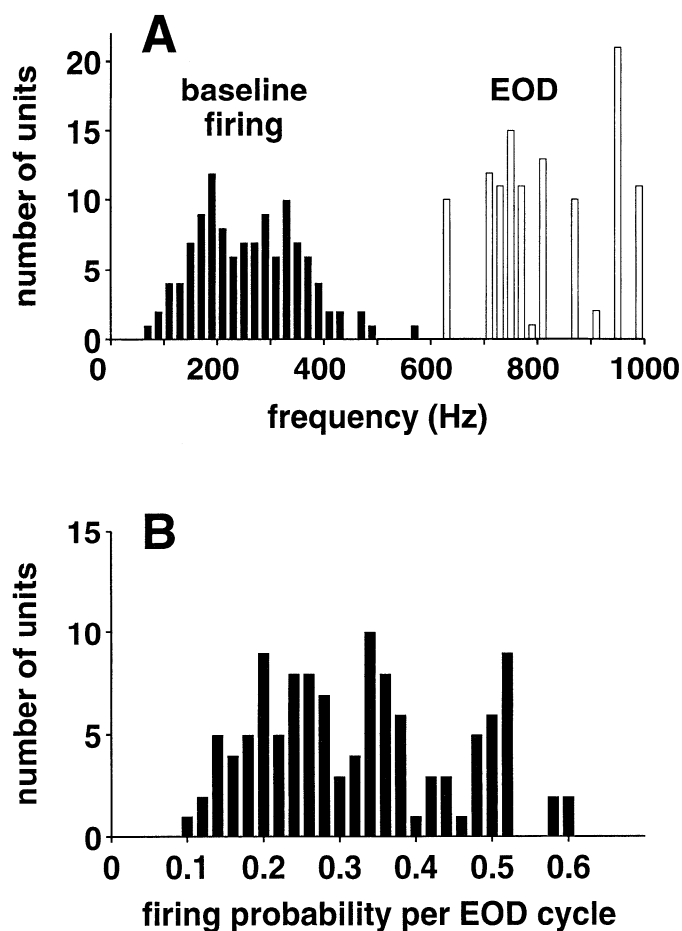
FIG. 1. Baseline firing characteristics of P-type afferents. A: distributions of baseline firing rates (solid bars) and electric organ discharge (EOD) frequencies (open bars) from 117 units in 11 fish. Each fish had a fixed EOD frequency corresponding to 1 of 11 open bars in the figure. Height of open bars reflects number of units per fish that were included in this sample. B: mean firing probability per EOD cycle (P) under baseline conditions.

FIG. 2. Baseline interspike interval (ISI) distributions and identification of bursty and nonbursty units. A: representative ISI distribution for a P-type afferent with a nonbursty firing pattern. Time interval between successive spikes is expressed in units of the EOD period (1 EOD period = 1.36 ms in this fish). B: representative ISI distribution for a bursty unit recorded from the same fish. Note significant number of intervals occurring at 1 EOD period. Insets in A and B show 100 ms samples of the corresponding afferent nerve recording (scale bar = 10 ms). Small, high-frequency oscillations in inset records are an artifact from EOD signal (frequency = 735 Hz). C: scatter plot used to classify afferents into bursty and nonbursty categories. Ordinate represents fraction of intervals that fall into first ISI peak centered at 1 EOD period. Abscissa represents the mean interspike interval for all intervals that do not fall into this first peak. Points corresponding to ISI distributions shown in A and B are labeled with corresponding letter. Units were classified as bursty if single-cycle fraction was larger than a cutoff $f_c = e^{-(x-1)^2/4} + 0.1$ (dashed curve). For a given range on abscissa, bursty units (●) have a larger fraction of single-cycle intervals than nonbursty units (○).

potentials (typically doublets and triplets), in which individual spikes in the cluster are separated by about one EOD cycle, whereas nonbursty units show no such clustering. We also observed these two types of firing patterns in our data as illustrated in Fig. 2, A and B, for a representative nonbursty and bursty unit, respectively. P-type afferents fire at most one spike per cycle, loosely phase-locked to the EOD cycle. Hence the interspike intervals cluster at multiples of the EOD period as illustrated by the interspike interval (ISI) histograms in Fig. 2. To classify units as bursty or nonbursty, we analyzed the fraction of interspike intervals falling in the single-cycle peak of the ISI histogram in relation to the mean interspike interval when these single-cycle events are excluded. For example, the nonbursty unit shown in Fig. 2A has a mean interspike interval of 5.3 EOD cycles and the fraction of intervals falling into the single-cycle peak of the ISI histogram is 0. The unit in Fig. 2B, which was recorded from the same fish, has 30% of the interspike intervals occurring in the first peak of the ISI histogram, and if these single-cycle intervals are excluded, the mean interspike interval for the remaining distribution is 4.7 EOD cycles. As illustrated in Fig. 2C, we classified units as bursty if the
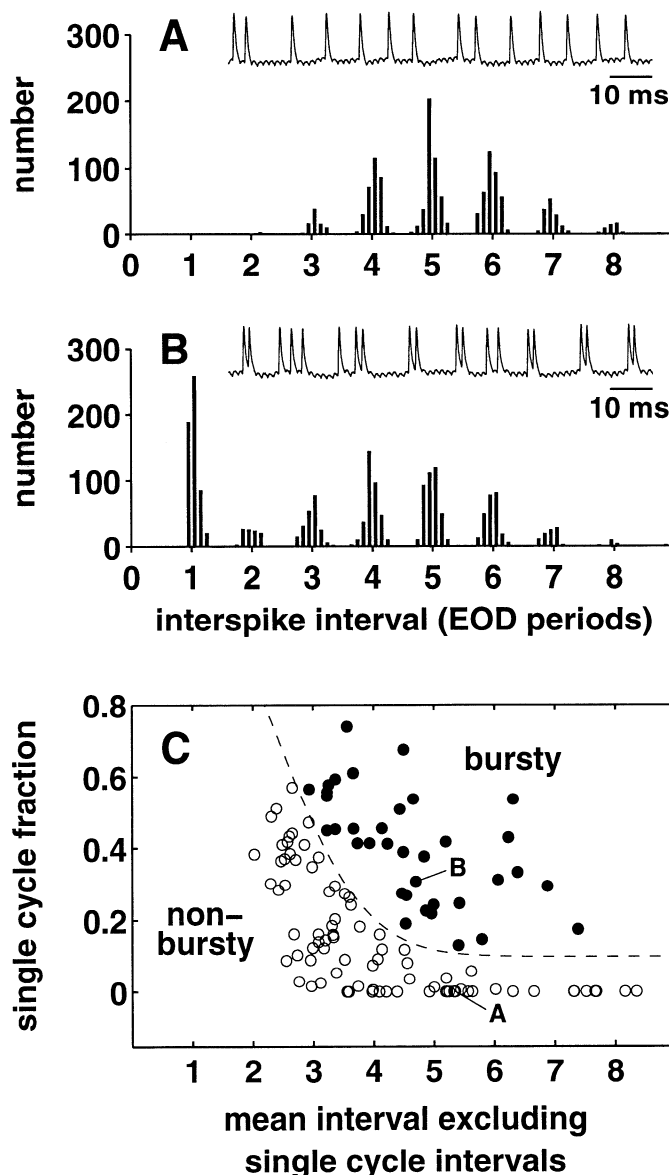
fraction of intervals falling in the single-cycle peak was larger than a cutoff (dashed curve) that reflected the expected fraction, based on the mean interspike interval of the remaining distribution. The cutoff fraction f_c was computed as $f_c = e^{-(x-1)^2/4} + 0.1$, where x is the mean interspike
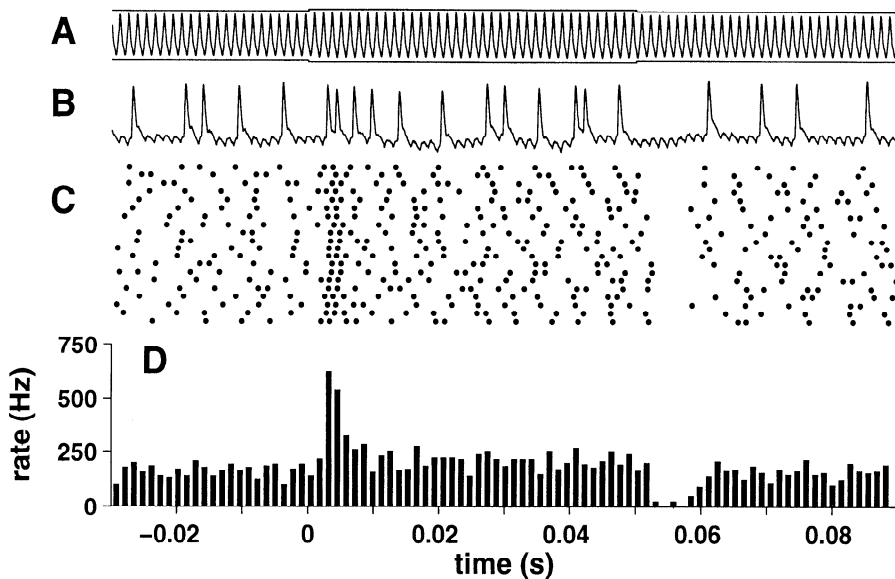
FIG. 3. Representative response of a P-type afferent to an amplitude-modulation (AM) step stimulus. *A*: recording of change in transdermal potential created by a small positive AM step stimulus. Stimulus amplitude in this case was −25 dB (0.056 mV rms), which corresponded to an increase of ~6% in baseline amplitude of carrier signal (0.89 mV rms). Horizontal lines above and below carrier signal represent the AM stimulus envelope. *B*: afferent nerve recording showing an increase in firing rate after onset ($t = 0$) of stimulus and a decrease in firing rate after offset ($t = 0.05$ s) of AM step. *C*: dot raster display of spike times for first 20 trials in a series of AM step stimuli presented with an intertrial interval of 1 s. *D*: peristimulus firing rate estimate constructed from an average of 100 trials (see METHODS).

interval excluding single-cycle intervals. This empirically determined cutoff function reflects the fact that single-cycle intervals become more common, even in nonbursty units, as the mean interspike interval decreases. Using this criterion, 31% of the afferents in this sample were categorized as bursty.

Responses of P-type afferents to AM steps

A typical response of a P-type afferent to a short duration AM step increase in the local transdermal potential is illustrated in Fig. 3. Before the step, afferent activity is at the baseline level. After the onset of the positive step ($t = 0$ s), the afferent responds with an abrupt increase in firing rate that subsequently declines back toward the baseline level. At the offset of the step ($t = 0.05$ s), the afferent rate decreases abruptly to 0 and subsequently returns to the baseline level. As illustrated by the raster display in Fig. 3*C*, the response elicited by a brief AM step stimulus is similar across repeated trials, provided that the intertrial interval is sufficiently long to allow the firing rate to recover to its baseline level before the next step stimulus is presented. Under these conditions, spike activity can be averaged across multiple trials to obtain an estimate of the instantaneous firing rate as shown by the peristimulus rate histogram in Fig. 3*D*. Note that there is a brief response delay of ~2.5 ms relative to the onset of the stimulus at $t = 0$ (this delay can be seen more clearly in Fig. 7*A*). As can be seen in the raster display in Fig. 3*C*, there is a slight variability in this onset delay from trial to trial.

The adaptation time course illustrated in Fig. 3*D* appears to be of a phasic-tonic nature, with an initial rapid decay over the first few time bins, followed by an apparent plateau that is slightly above the baseline firing level. An interesting property of P-type afferent adaptation is that qualitatively similar response profiles can be observed on multiple time scales. Figure 4, *A–C*, illustrates the multiscale characteristics of P-type afferent adaptation in response to a prolonged AM step stimulus lasting 100 s. When the initial 1 s of the

response is viewed on a linear time scale (Fig. 4*A*), the adaptation time course appears to involve an initial decay in the first few hundred milliseconds followed by a plateau. However, when the same data is viewed on a 10 s time scale (Fig. 4*B*), adaptation now appears to take place over several seconds, again followed by an apparent plateau. Finally, when the full data record is viewed on a 100-s time scale (Fig. 4*C*), even slower components of the adaptation over the first tens of seconds can be observed. Given the multiple time scales that appear to be involved in P-type afferent adaptation, it is more informative to examine the data on a logarithmic time scale as shown in Fig. 4*D*. This representation clearly shows that the afferent response continues to adapt throughout the duration of the 100-s step stimulus.

All P-type afferent fibers showed a time course of sensory adaptation in response to AM step stimuli similar to that in Fig. 4. Figure 5*A* shows a logarithmically binned population average of the normalized firing rate change in 49 units (11 fish) for which we obtained stable recordings lasting more than 100 s in response to positive AM step stimuli. Individual responses, similar to that shown in Fig. 4*D*, first were rescaled to give a normalized response amplitude $r_{norm}(t)$ of 1.0 at $t = 1$ s, then the rescaled values were averaged across the population of units to obtain the mean normalized response $\langle \Delta r_{norm}(t) \rangle$. The error bars in Fig. 5*A* represent the standard deviation of the population average, which is typically less than ~10–20% of the mean, reflecting a high degree of similarity in the adaptation time course for all units. Due to the logarithmic spacing, the first few bins of both the step response data (●) and the baseline control runs (○) contain only a small number of spikes, thus leading to larger statistical fluctuations in those bins.

Parameterizing the adaptation time course

As illustrated in Fig. 5*B*, the inverse of the mean normalized response $1/\langle \Delta r_{norm}(t) \rangle$ yields an approximately straight line when plotted on a logarithmic time scale. This linear relationship suggested a parameterization for the normalized
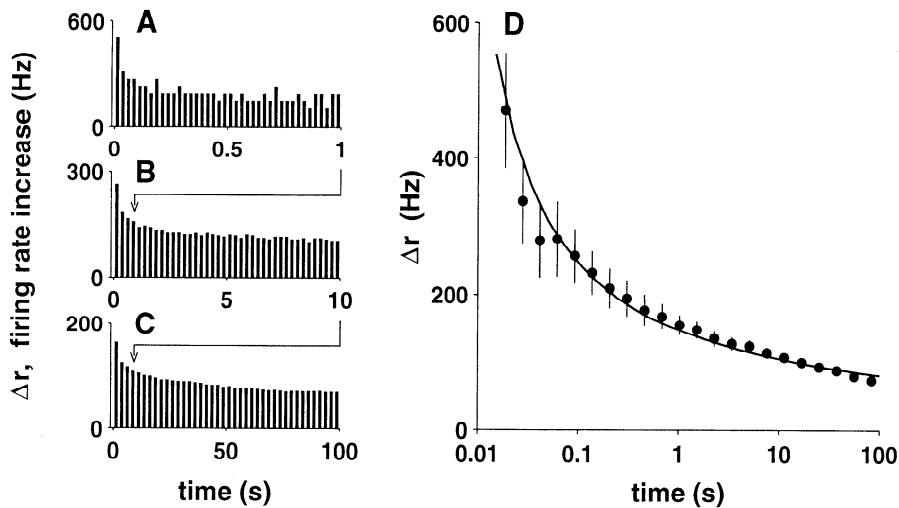
FIG. 4. Time course of sensory adaptation in response to a single presentation of a long duration (100 s) AM step stimulus viewed on multiple time scales. A: poststimulus firing rate increases (rate above baseline) for first 1 s of afferent response viewed on a linear time scale; bin width = 0.025 s. B: first 10 s of same response; bin width = 0.25 s. C: first 100 s of response; bin width = 2.5 s. Note that increase in firing rate appears to reach a plateau level by end of records in A and B, but when viewed on a longer time is actually continuing to decline (arrows). D: time course of sensory adaptation viewed on a logarithmic time scale. Error bars reflect statistical error on rate estimate based on number of spikes in each bin. Solid curve is a least squares fit to data using functional form: $\Delta r(t) = A/[B \ln (t) + 1]$ with best-fit parameter values of $A = 148$ and $B = 0.17$.

response data of the form $1/\langle \Delta r_{norm}(t) \rangle = B \ln (t) + 1$, where the parameter B determines the slope. The line is constrained to pass through a value of 1.0 at $t = 1$ s by the normalization procedure. The solid line in Fig. 5B is the result of a least squares fit that resulted in a best-fit value of $B = 0.143$. Inverting the relationship to yield $\langle \Delta r_{norm}(t) \rangle = 1/[B \ln (t) + 1]$ produces the solid curve in Fig. 5A, which provides a good description of the normalized adaptation time course averaged over the population. For comparison, fits of the form $\langle \Delta r_{norm}(t) \rangle = t^{-k}$ and $\langle \Delta r_{norm}(t) \rangle = \ln (1 + \lambda/t)/\ln (1 + \lambda)$ also are shown in Fig. 5A. These latter forms are described in DISCUSSION.

To test whether or not the logarithmic parameterization is capable of providing a good description of individual responses and not just of the population average, we performed least squares fits to the time course data for each of the 49 units included in the population average using the following form:

$$\Delta r(t) = A/[B \ln (t) + 1] \qquad (1)$$

where Δr is the firing rate change relative to the baseline level, A is an amplitude parameter with units of spikes/s, B is the dimensionless slope parameter introduced above, and t is the time relative to the onset of the AM step stimulus in seconds. Figure 6 summarizes the best-fit parameter values for A and B. A representative fit to an individual response is illustrated in Fig. 4D. The mean χ^2 value for the fits was 22.4 ± 46.8 ($n = 49$) with 22 degrees-of-freedom (ν). Five of the fits had P values <0.001, indicating that the deviations between the data and the fit were statistically significant; all other fits were statistically consistent with the data. The units with small P values typically exhibited some sort of "kink" or "bump" in the adaptation time course that contributed to the large χ^2 value. The characteristics of these occasional irregularities varied among the five units and we suspect that they are not intrinsic properties of the step response.

The distribution of best-fit values for the parameter A (Fig. 6A) had a mean of 105 ± 43 spikes/s ($n = 49$). As seen from Eq. 1, the parameter A corresponds to the firing rate change Δr at time $t = 1$ s. Thus the mean increase in firing rate one second following the onset of an AM step stimulus was typically ~ 100 spikes/s. This particular value

is not a fundamental property of P-type afferents, but arises from our attempts during the recording session to select a stimulus intensity for each afferent that produced a substantial change in firing rate, but one which was not so strong as to drive the unit into firing rate saturation. Responses from several units that were inadvertently driven into saturation during the initial portion of the response were excluded from the population average response shown in Fig. 5 and from the least squares fits presented here.

The distribution of best-fit values for the parameter B (Fig. 6B) had a mean of 0.149 ± 0.028 ($n = 49$), in good agreement with the value of 0.143 obtained from the fit to the population-averaged response in Fig. 5B. The temporal derivative of Eq. 1, $d(\Delta r)/dt$, evaluated at $t = 1$ s is equal to $-AB$. Thus the slope of the adaptation curve (on a linear scale) one second following the onset of an AM step stimulus was typically around -15% of the amplitude of the response at the point. For example, responses with a mean value Δr of 100 spikes/s at $t = 1$ s, typically had a slope of about -15 (spikes/s)/s at that point in the adaptation time course.

We observed a modest correlation between the best-fit values of A and B ($r = 0.26$), but the correlation value is only marginally significant ($P = 0.07$, $n = 49$). Part of the basis for the observed correlation may be that low-amplitude responses (small A), are more likely to appear to have a flatter adaptation time course (small B) due to statistical fluctuations in the number of spikes in the first few bins of the response. This may be the case for the two units that have B values <0.1 and appear to lie outside the main distribution (Fig. 6B). If we exclude units with an amplitude parameter A <80, we find almost no residual correlation between A and B for larger amplitude responses ($r = 0.04$, $n = 33$), even though the distribution of A still spans a wide range of values (from 81 to 229 spikes/s). Thus it appears that the time course parameter B is largely independent of the response amplitude.

To determine whether or not bursty and nonbursty units differed in their adaptation time course, we compared the distributions of the parameters A and B for these two subpopulations (see Fig. 2C). We found no significant differences between the mean parameter values for these two groups
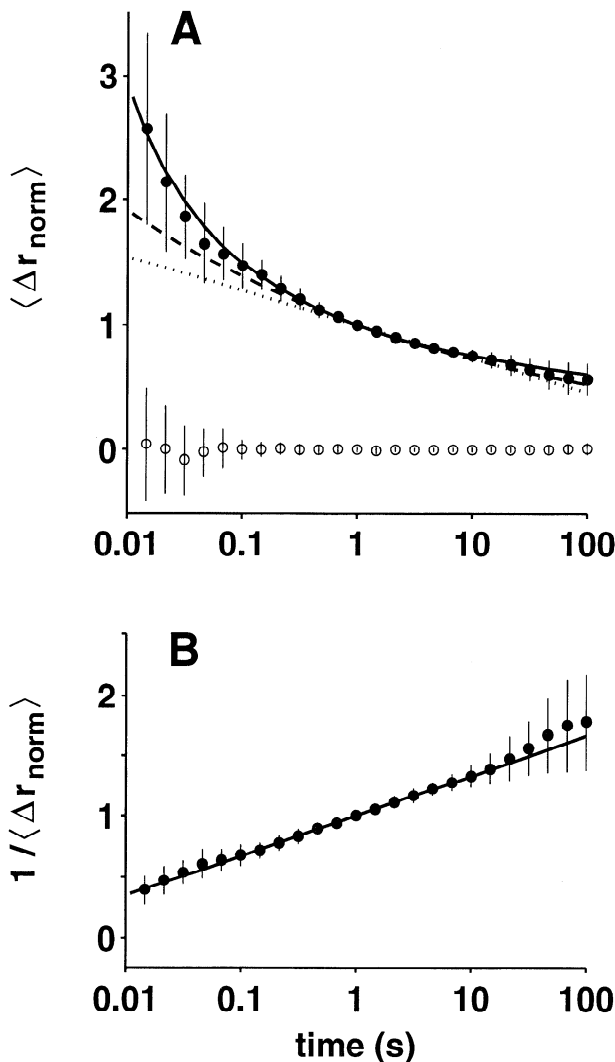
Δr on very short time scales required the use of short duration step stimuli with large numbers of repeated trials. Figure 7A shows the first 10 ms of the step response from a single afferent recording shown previously in Fig. 3D. The change in firing rate Δr, computed from an average of 100 trials, is plotted on a linear scale using a bin width equal to the EOD period (1.35 ms). There is a response delay t_r between the onset of the step stimulus at $t = 0$ and the onset of the response ~2.5 ms later, which is due to the combined effects of synaptic and propagation delays. The change in firing rate for $t > t_r$ is well described by $\Delta r(t) = A/[B \ln (t - t_r) + 1]$ with $A = 10.8$, $B = 0.18$. The fit prediction is plotted in a staircase fashion, rather than a smooth curve to reflect the fact that these values were computed for discrete times corresponding to individual EOD cycles. Thus the logarithmic form appears to provide a reasonable description of the adaptation time course on time scales as short as the first few EOD cycles of the response.

To evaluate the logarithmic form on time scales >100 s, we analyzed step response data from six afferents for which we obtained stable recordings lasting >600 s. Figure 7B shows a population average of the normalized firing rate
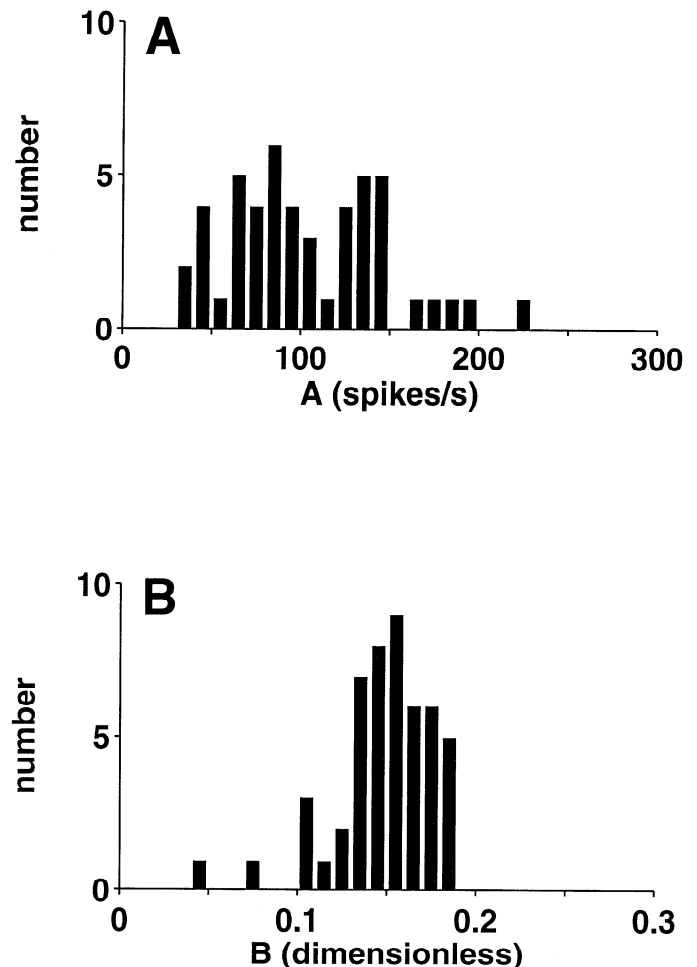
FIG. 5. Population-averaged time course of sensory adaptation. A: mean normalized firing rate increase $\langle \Delta r_{norm} \rangle$ in response to long duration (>100 s) AM steps (●). Error bars represent standard deviation of population average; standard error of mean for each data point is a factor of 7 smaller. Average of 26 control responses with no AM step stimulation (○) shows a flat baseline centered on 0. B: inverse mean normalized firing rate $1/\langle \Delta r_{norm} \rangle$ varies approximately linearly with logarithm of time. Solid curves in A and B are results of a least squares fit to population averaged inverse mean firing rate using logarithmic form $\langle \Delta r_{norm}(t) \rangle = 1/[B \ln (t) + 1]$ with a best-fit parameter value $B = 0.143$. Dashed curve in A is a fit of form $\langle \Delta r_{norm} \rangle = t^{-k}$ with $k = 0.141$. Dotted curve is a fit of form $\langle \Delta r_{norm} \rangle = \ln (1 + \lambda/t)/\ln (1 + \lambda)$ with $\lambda = 4,960$ s. Latter 2 functional forms, which do not fit early part of response as well as logarithmic form, are described in DISCUSSION.

using the Student's t-test (bursty: $A = 104.7 \pm 50.4$, $B = 0.150 \pm 0.025$; nonbursty: $A = 104.5 \pm 38.9$; $B = 0.148 \pm 0.03$). Thus bursty and nonbursty P-type afferents can be considered as a homogeneous population in terms of their adaptation time course.

Adaptation on shorter and longer time scales

Most of our experiments were designed to cover the time range from 10 ms to 100 s as summarized in Fig. 5. However, we also acquired some data that can be used to evaluate the logarithmic form on shorter ($t < 10$ ms) and longer ($t > 100$ s) time scales. To accurately evaluate the rate change

FIG. 6. Best fit parameter values for fits of form $\Delta r(t) = A/[B \times \ln (t) + 1]$ to individual long-duration (>100 s) AM step responses. Individual responses and fit results are similar to that shown in Fig. 4D. A: parameter A characterizes amplitude of response. B: dimensionless parameter B characterizes time course of response.

varying amplitudes. Figure 8A shows a response series from one representative unit using positive and negative AM steps with absolute stimulus amplitudes ranging between −5 and −20 dB in 5-dB increments. When the responses in Fig. 8A were fit using the logarithmic form, the best-fit values of A were found to vary linearly with stimulus amplitude, as illustrated in Fig. 8B. For large AM step increases, P-type afferents can be driven into firing rate saturation where the afferent fires one spike per EOD cycle during the initial portion of the response, and hence has an initial firing rate equal to the EOD frequency (*inset,* Fig. 8A). For large AM step decreases, afferents can be driven into firing rate rectification in which the unit has a 0 firing rate during the initial portion of the response, as illustrated by the largest-
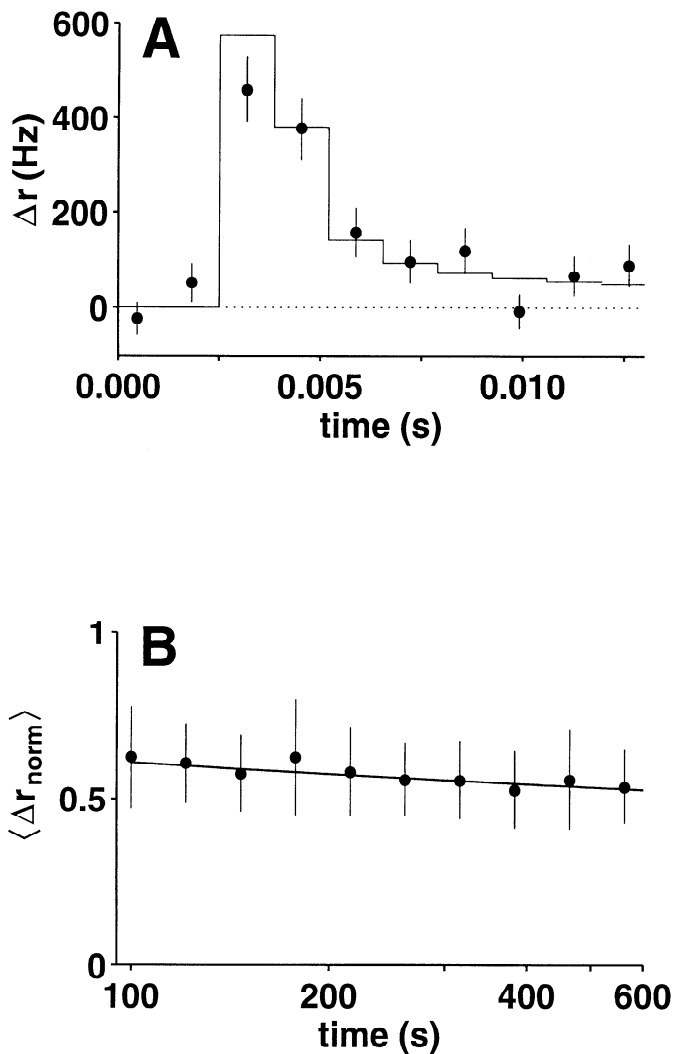

FIG. 7. Evaluation of logarithmic form on shorter ($t < 0$ ms) and longer ($t > 100$ s) time scales than shown in Fig. 5. *A*: short time scale analysis showing first 10 ms of AM step response data from Fig. 3D using a bin width equal to EOD period (1.35 ms). Experimental measurements are shown (●) with error bars. Solid line is a fit using logarithmic form as described in text. *B*: long-term firing rate change in response to prolonged AM steps for 6 afferents in which stable recordings were obtained for durations exceeding 600 s (only portion of response for $t > 100$ s is shown). Error bars represent standard deviation of population average for each bin. Solid curve corresponds to $\langle \Delta r_{norm}(t) \rangle = 1/[B \ln(t) + 1]$ with $B = 0.14$.

change in these six units, using the same normalization procedure introduced earlier. Responses were first rescaled to give a normalized response amplitude $r_{norm}(t) = 1.0$ at $t = 1$ s, then the normalized values were averaged across the population of six units. The decrease in mean normalized firing rate of ~13% over the time period between 100 and 600 s is well described by $\langle \Delta r_{norm} \rangle = 1/[B \ln(t) + 1]$ with $B = 0.14$. Thus we see that the logarithmic form is also capable of describing very slow components of the adaptation time course.

Response linearity

To evaluate the dependence of the parameter A in *Eq. 1* on stimulus amplitude, we recorded responses from several units using series of AM step increases and decreases of
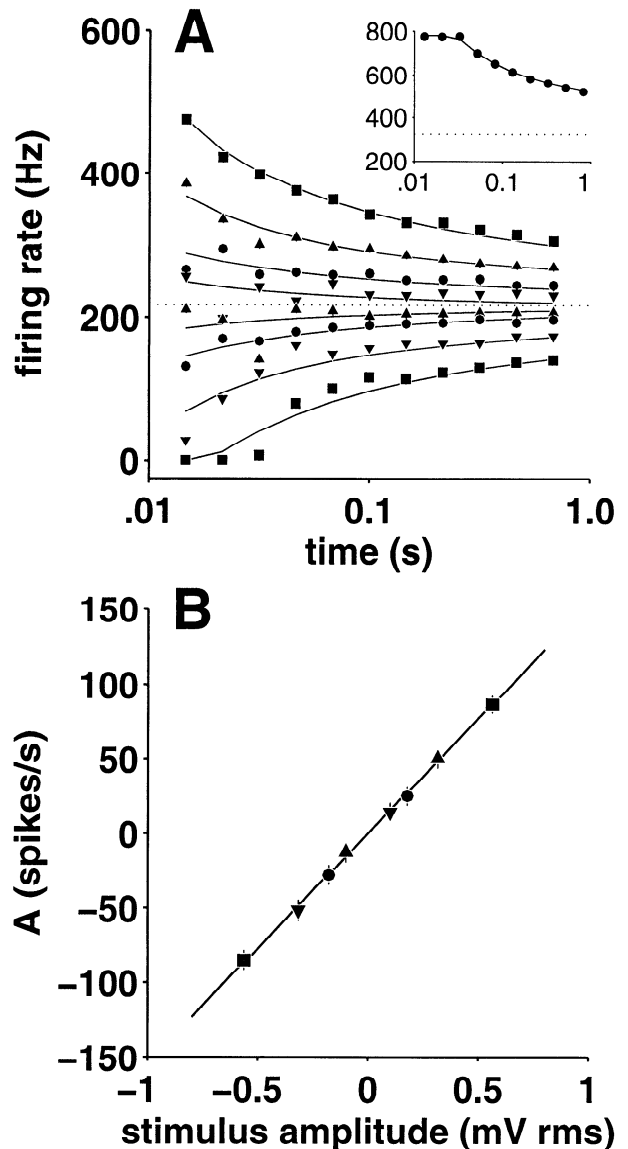

FIG. 8. Linearity of P-type afferent responses with respect to stimulus amplitude. *A*: series of response profiles to AM step increases and step decreases with amplitudes ranging between −5 dB (0.56 mV rms) and −20 dB (0.10 mV rms) in 5-dB steps. Solid lines are logarithmic fits using *Eq. 1* with additional constraints for firing rate rectification and saturation (see text). An example of a saturated response is shown (*inset*). Dotted lines represent baseline firing rate. *B*: amplitude of afferent response, characterized by best-fit parameter value A, depends linearly on stimulus amplitude.

amplitude step decrease (-5 dB) in Fig. 8A. To take these clipping nonlinearities into account in our fitting procedure, we added additional constraints to Eq. 1 that prevented the predicted firing rate from taking on values <0 or larger than the EOD frequency: $0 \leq r(t) \leq f_{EOD}$. In terms of the rate change Δr relative to the baseline level, these constraints take the form: $-r_{base} \leq \Delta r(t) \leq f_{EOD} - r_{base}$. Except for the effects of these clipping nonlinearities, we found that P-type afferent responses scaled linearly with stimulus amplitude over the range of amplitudes tested.

Frequency domain response characteristics

For a linear system, the step response can be used to predict the frequency domain response characteristics of the system. Assuming response linearity, we computed the gain and phase characteristics of the modulation transfer function for P-type afferents from the logarithmic parameterization of the step response. As illustrated in Fig. 9, the predicted gain and phase characteristics are able to provide a good fit to measured P-type afferent responses to sinusoidal AM stimuli over a range of AM frequencies from 1 to 100 Hz. The data points in Fig. 9 were obtained from 1 representative unit out of 16 P-type afferents, which were characterized in an earlier study of P-type afferent AM frequency response characteristics (Xu et al. 1994). The logarithmic parameterization of the adaptation time course in the time domain thus appears to accurately capture the frequency domain response dynamics of P-type afferents over a wide range of behaviorally relevant AM frequencies.

DISCUSSION

A new functional form for describing sensory adaptation

We have introduced a new functional form for describing the time course of spike frequency adaptation in sensory systems: $\Delta r(t) = A/[B \ln (t) + 1]$, where Δr is the change in firing rate relative to the pre-stimulus level, A is a parameter that characterizes the amplitude of the response, B characterizes the time course of the response, and t is time relative to the onset of a maintained step stimulus. This logarithmic form successfully describes the time course of sensory adaptation in P-type electrosensory afferents in *A. leptorhynchus* over five decades in time, from milliseconds to hundreds of seconds, using just two free parameters. This is the first time that the adaptation time course of electrosensory afferents has been quantitatively described in this particular species of weakly electric fish. We strongly suspect that the logarithmic adaptation time course we observed is not peculiar to this species but is likely to be a general property of electrosensory afferent adaptation in gymnotid species with wave-type EODs. There have been several previous studies of P-type afferent adaptation in related gymnotid species (Hagiwara et al. 1965; Hopkins 1976; Scheich et al. 1973; Shumway and Maler 1989). These studies have reported adaptation time constants ranging from 0.2 to 3.4 s and also have reported that the time constants appeared to show a great deal of variability (Hopkins 1976). We believe that the wide range and variability of previously reported time constants arises from attempts to describe a logarithmically decaying function in terms of exponentially decaying components. As
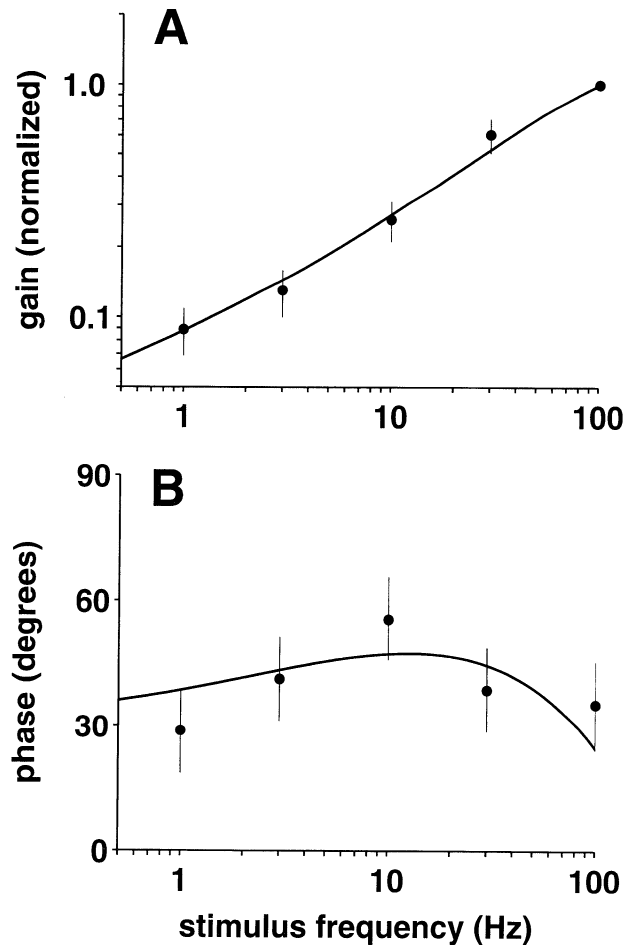

FIG. 9. Frequency domain response characteristics of P-type afferents. Data points are from an analysis of response of an individual afferent nerve fiber to sinusoidal AM stimulation with AM frequencies ranging between 1 and 100 Hz (Xu et al. 1994). Error bars represent uncertainty in best-fit amplitude and phase parameters obtained from least squares fits to AM response data. Solid curves represent predicted frequency response derived from logarithmic parameterization of step response $\Delta r(t) = A/[B \ln (t) + 1]$ with $B = 0.147$. *A*: normalized gain of afferent response vs. AM frequency. Gain has been normalized to 1.0 at maximum response amplitude. *B*: phase of response versus AM frequency. A positive value of phase indicates that response leads stimulus.

discussed below, fitting exponentials to the adaptation time course can lead to apparent time constants that depend upon multiple factors, including the duration of the response that is analyzed, the bin width that is used, and whether or not the unit was driven into firing rate rectification or saturation by the stimulus. In contrast, the results of fits using the logarithmic form of Eq. 1 are largely insensitive to these factors.

Comparison with exponential forms

One common approach to parameterizing the time course of sensory adaptation is to characterize the change in firing rate Δr in terms of one or more exponentially decaying components using the general form

$$\Delta r(t) = A_1 e^{-t/\tau_1} + A_2 e^{-t/\tau_2} + \cdots + A_n e^{-t/\tau_n} + C \quad (2)$$

where A_i are amplitude coefficients, τ_i are time constants, and C is an optional constant term for fitting the tonic compo-

nent of a phasic-tonic (partially adapting) response profile. Previous reports of the adaptation time course in gymnotid P-type afferents have assumed, either implicitly or explicitly, that it could be described in this form using one or two time constants plus a tonic term (Hagiwara et al. 1965; Hopkins 1976; Scheich et al. 1973; Shumway and Maler 1989).

Because of the multiscale nature of the actual adaptation time course, which involves time scales ranging from milliseconds (Fig. 3D) to tens of seconds (Fig. 4C), a multiexponential parameterization of P-type afferent adaptation requires several time constants to adequately describe the full adaptation time course. A multiexponential fit to the population averaged response in Fig. 5A using Eq. 2 required a total of nine free parameters (4 time constants, 4 corresponding amplitude parameters, and 1 tonic response term) to produce a fit with a χ^2 per degree-of-freedom comparable with that obtained with the two-parameter logarithmic form of Eq. 1. A four-exponential fit to the full 100-s record length in Fig. 5A produced the following best-fit time constants: $\tau_{1-4} = (0.013, 0.193, 1.50, 23.6\ s)$. A similar fit that only included the first 10 s of the response data in Fig. 5A resulted in a different set of time constants: $\tau'_{1-4} = (0.011, 0.132, 0.574, 3.99\ s)$. Because there are not any significant shoulders or inflections in the adaptation time course, the time constants are not constrained by any particular feature of the response profile, but rather redistribute across the available time range to give the best approximation to the data.

Similar variability arises when the bin widths or sampling intervals used in estimating the instantaneous firing rates are altered. For example, a biexponential fit to the response data in Fig. 4B (10-s record length, 0.250-s bin width) yields best-fit time constants of 0.238 and 3.71 s. A fit to the same data sample using bins that are half as wide yields time constants of 0.120 and 2.39 s. Another source of variability in exponential fits occurs when units are driven into rectification (0 firing rate) or saturation (firing at the EOD frequency) by the stimulus. These clipping nonlinearities mask the fastest components of the adaptation, causing a systematic shift in the best-fit time constants to longer values.

Because the results obtained from multiexponential fits to P-type afferent adaptation are subject to these many sources of variability, it would be misleading to interpret the resulting time constants as reflecting fundamental properties of afferent response dynamics corresponding to underlying biophysical mechanisms. The time constants obtained from multiexponential fits to P-type afferent data should be thought of as terms in a series expansion in which exponentials are used as a basis set for approximating the actual time course, which in this case appears to be of a logarithmic form. This is not to say that multiexponential fits are necessarily just an approximation in all sensory systems. In cockroach tactile spines, for example, sensory adaptation is well described by three exponential processes with discrete time constants (French and Torkkeli 1994).

Comparison with power law and related forms

Sensory adaptation occurring on multiple time scales, similar to that described here for P-type afferents, has been reported in other sensory systems and the adaptation time course in these cases has often been parameterized using a power law form (review: Thorson and Biederman-Thorson 1974)

$$\Delta r(t) = At^{-k} \tag{3}$$

where A is an amplitude parameter, $0 < k < 1$ is a fractional exponent that characterizes the adaptation time course and t is the time relative to the onset of a step stimulus. Like the logarithmic form in Eq. 1, the power law form in Eq. 3 involves only two free parameters. There is a close correspondence between the interpretation of the parameters A and B in the logarithmic form and the parameters A and k in the power law form. For both forms, the firing rate change Δr at time $t = 1$ s is equal to A. The slope of the response, $d(\Delta r)/dt$, at $t = 1$ s is equal to $-AB$ for the log form and $-Ak$ for the power law form. Thus for the same value of A and with $B = k$, the logarithmic and power law forms both pass through the same point with the same slope at $t = 1$ s. For times <1 s, the log form has a steeper slope, whereas for times >1 s, it has a more gradual slope. Because of these differences, particularly at short time scales, the logarithmic form does a better job than the power law form at describing the adaptation time course for P-type afferents. Figure 5A shows a comparison between a log form fit (solid line) and a power law fit (dashed line) to the mean normalized adaptation time course. Best-fit parameter values are $B = 0.143$ for the log form and $k = 0.141$ for the power law form. The χ^2 per degree-of-freedom is significantly different for the two fits, with a value of $\chi^2/\nu = 2.0$ for the log fit and $\chi^2/\nu = 10.2$ for the power law fit. The early components of the response are not well described by the power law form, but after the first few hundred milliseconds, the power law and logarithmic forms give comparable fits.

Another functional form for sensory adaptation has been proposed by Norwich and McConville (1991) based on information theoretical considerations pertaining to the uncertainty or entropy associated with measurements of stimulus intensity by sensory receptors. For constant stimulus intensity, this informational form can be written as

$$\Delta r(t) = A \ln(1 + \lambda/t) \tag{4}$$

where A is an amplitude parameter, λ is a parameter that determines the adaptation time course, and t is time relative to stimulus onset. When t is large ($t \gg \lambda$), a Taylor series expansion yields $\Delta r(t) \approx A\lambda t^{-1}$, hence this form asymptotically converges to a power law form t^{-k} with $k = 1$. When Eq. 4 is normalized to give a rate change $\Delta r = 1$ at $t = 1$ s, it takes the form $\Delta r = \ln(1 + \lambda/t)/\ln(1 + \lambda)$. Figure 5A shows a fit of this form to the normalized adaptation time course (dotted line) with a best fit parameter value $\lambda = 4,960$ s. This form, like the power law form, does a reasonable job of describing the long time scale portion of the response but produces an even poorer fit to the first few hundred milliseconds of the response data.

Frequency domain analysis and fractional order dynamics

The power law form for sensory adaptation in Eq. 3, which varies as t^{-k} in the time domain, has a frequency domain transfer function that varies as s^k, where s is the complex frequency [$s = i(2\pi f)$; f = frequency, $i = \sqrt{-1}$] (Thorson and Biederman-Thorson 1974). Recall that in the formula-

tion of the power law form for sensory adaptation (*Eq. 3*), k takes on fractional values in the range between 0 and 1. Thus the s^k dependence in the frequency domain is often described in terms of fractional order dynamics or fractional order filtering (Thorson and Biederman-Thorson 1974). This form has been used to describe sensory filtering in several sensory systems, including ampullary electroreceptors in the catfish (Bretschneider et al. 1985).

Sensory adaptation in the time domain corresponds to high-pass filtering in the frequency domain. A simple first-order high-pass filter has a step response $e^{-t/\tau}$ in the time domain and a transfer function $s/(s + 1/\tau)$ in the frequency domain. Far below the knee of the transfer function, which occurs at $f = 1/(2\pi\tau)$, the gain of a first-order filter is approximately proportional to frequency and has a roll off of 20 dB per decade. In contrast, a fractional order filter with a transfer function of s^k has a more gradual roll off and no knee. For $k = 0.141$, which was the value we obtained for the power law fit to P-type afferent adaptation in Fig. 5A, we would expect a roll off of only 2.8 dB per decade if P-type afferent adaptation obeyed the power law form. However, as seen in Fig. 9, the actual roll off for P-type afferents is closer to 10 dB per decade, which is inconsistent with the prediction from the power law fit to the time domain data. This discrepancy arises because the power law form underestimates the initial rapid decline in firing rate over the few hundred milliseconds of the response (Fig. 5A). The logarithmic form, on the other hand, provides a consistent description in both the time domain (Fig. 5) and the frequency domain (Fig. 9), thus providing further evidence that the logarithmic form produces a better characterization of P-type afferent response dynamics than the power law form.

Summary of alternative functional forms

Our critiques of the fits produced by multiexponential (*Eq. 2*), power law (*Eq. 3*), and informational (*Eq. 4*) forms for parameterizing the adaptation time course are made relative to our P-type afferent response data. These other functional forms are certain to do a better job than the logarithmic form (*Eq. 1*) for characterizing sensory adaptation in some systems. We do not wish to leave the impression that we believe the logarithmic form should be universally better than these other forms as a parameterization for sensory adaptation. The importance of our results is to emphasize that one should avoid making a priori assumptions about the functional form that adaptation should take in any sensory system until the data have been analyzed carefully. Most of the functional forms that we have introduced (*Eqs. 1–4*) are capable of approximating one another to a reasonable degree of accuracy over some restricted range of time values. Thus it is often possible to achieve reasonable fits, as judged by a χ^2 per degree-of-freedom criterion, using more than one of these forms, but only the form that most accurately describes the full adaptation time course will prove useful for extrapolating outside the range of the fit.

Singularity in the logarithmic form

It is interesting to examine the behavior of the various functional forms in *Eqs. 1–4* for small time values. In the limit as t approaches 0, the rate change Δr in the multiexponential form (*Eq. 2*) assumes a finite value, whereas both the power law (*Eq. 3*) and informational forms (*Eq. 4*) have singularities at $t = 0$, such that Δr approaches infinity as t approaches 0. The logarithmic form (*Eq. 1*) is unique in that it has a singularity at a nonzero value of t. The singularity occurs as t approaches a value of $e^{-1/B}$ and the denominator, $B \ln(t) + 1$, therefore approaches 0. Using a value of $B = 0.149$ from the mean of the distribution in Fig. 6B, we find that this singularity typically occurs in our fits near a value of $t = 0.0012$ s. Interestingly, this value is very close to the mean EOD period ($t_{EOD} = 1/f_{EOD}$) of 0.0013 s for units in our data sample, indicating that the singularity in the log form typically occurs near the first EOD cycle of the response. The fact that P-type afferents fire at most one spike per EOD cycle introduces a natural discretization of the time scale for observing changes in afferent firing rate. The logarithmic form is not intended to predict changes in firing rate on time scales shorter than one EOD cycle, thus the negative firing rate changes obtained from *Eq. 1* for $t < e^{-1/B}$ are considered as falling outside the domain of applicability. In terms of the underlying biophysics, one could certainly pose questions concerning processes occurring on time scales shorter than one EOD cycle, but we do not expect the logarithmic form to provide meaningful guidance in this domain.

Implications for the biophysical basis of sensory adaptation

The logarithmic parameterization of the adaptation time course for P-type afferents is a phenomenological description of the overall input-output relationship for a complex sensory encoding process. Receptor organs each contain multiple electroreceptor cells embedded in a canal structure that contributes to the temporal filtering properties of the organ (Bennett et al. 1989). Several receptor cells communicate with a single afferent nerve fiber via chemically mediated synaptic transmission, which in turn involves multiple subprocesses controlling the synthesis, storage, release, reuptake, and binding of neurotransmitter. Thus there are potentially a large number of biophysical processes, both pre- and postsynaptically, that could contribute to sensory adaptation in this system. Despite providing a good phenomenological description, the logarithmic form (*Eq. 1*) does not directly shed much light on which particular biophysical mechanisms contribute to the adaptation process. Because P-type afferent adaptation appears to involve time scales ranging continuously from milliseconds (Fig. 3D) to hundreds of seconds (Fig. 7B), it does not seem likely that adaptation could be explained by a few first-order biophysical processes with discrete time constants. It is more likely that adaptation in this system involves multiple spatially distributed and temporally distributed relaxation processes covering a wide range of time constants, as has been proposed as a basis for power law adaptation (Thorson and Biederman-Thorson 1974). One might hope to gain insights about underlying mechanisms from related vertebrate octavolateral systems (auditory, vestibular, and lateral line), but the biophysical mechanisms that contribute to sensory adaptation in these systems have not been fully identified either.

In mammalian auditory nerve fibers, for example, it is known that adaptation to sustained tones involves at least three time scales: rapid adaptation on the scale of milliseconds, short-term adaptation on the scale of tens of milliseconds, and slow adaptation on the scale of seconds. No adaptation is observed in the inner hair cell receptor potentials, therefore the biophysical basis of adaptation in the auditory system is presumed to primarily involve processes occurring at the synaptic level (reviews: Mountain and Hubbard 1996; Ruggero 1992).

Implications for central electrosensory processing

An accurate characterization of afferent response dynamics is essential for interpreting neural responses in later stages of electrosensory processing in the central nervous system and for building up computational models of information processing and adaptive sensory filtering in this system. The first stage of central electrosensory processing occurs in a medullary sensory nucleus called the ELL, which has several structural and functional similarities to the mammalian dorsal cochlear nucleus (Montgomery et al. 1995). The principal neurons of the ELL are pyramidal cells that receive primary afferent input from P-type afferents, either directly (E cells) or indirectly (I cells) via inhibitory interneurons and are the main projection neurons conveying amplitude-related information to higher centers. A major focus of ongoing research is to understand the role of feedback pathways in modulating the gain and spatiotemporal filtering properties of ELL pyramidal cells (Bastian 1986a,b; Bastian and Bratton 1990; Bratton and Bastian 1990; Nelson 1993, 1994a,b; Shumway and Maler 1989).

There have been several previous studies of ELL pyramidal cell adaptation, most of which have reported adaptation time constants in the range of ~25–75 ms (Bastian 1981b, 1986a; Shumway 1989; Shumway and Maler 1989). Bastian and Courtright (1991) carried out a systematic study of the correlation between pyramidal cell adaptation time constants and pyramidal cell dendritic morphology, and, as in earlier reports, they observed fast components of sensory adaptation in the range of tens of milliseconds when they used short-duration (100 ms) AM step stimuli. However, they also characterized pyramidal cell adaptation using much longer step stimuli (10-s duration) than had been used in previous studies. When they did so, they observed much slower components of pyramidal cell adaptation in the range of –0.5–4.0 s. This multiscale behavior—that longer adaptation time constants become apparent when longer record lengths are analyzed—is characteristic of the logarithmic adaptation time course of P-type afferents (see Fig. 4, *A–C*) and may be a feature of ELL pyramidal cell adaptation as well.

The multiscale nature of sensory adaptation in the gymnotid electrosensory system may have led inadvertently to a misconception regarding the relationship between afferent and ELL pyramidal cell adaptation rates. In most earlier studies, afferent adaptation has been characterized using long steps of several seconds in duration, whereas pyramidal cell adaptation has been characterized using much shorter duration stimuli. Consequently, most previous studies have reported significantly longer time constants for afferents than for pyramidal cells, leading to the conclusion that pyramidal cells exhibit a 23-fold (Shumway and Maler 1989) to 100 fold (Bastian 1986b) increase in adaptation rate relative to that of receptors. The results of Bastian and Courtright (1991) demonstrating slow components of pyramidal cell adaptation, together with our results showing very fast components of P-type afferent adaptation (e.g., Figs. 3*D* and 4*A*) suggest that this view needs to be reevaluated. Meaningful comparisons between P-type afferent and ELL pyramidal cell adaptation will require a careful reanalysis of the pyramidal cell adaptation time course.

Implications for descending gain control

Bastian and Bratton (1990) described a class of multipolar neurons in the nucleus praeeminentialis pars dorsalis (NPd) of *A. leptorhynchus*; these appear to show a tonic response to the mean amplitude of the transdermal potential established by the EOD. These NPd multipolar neurons form part of a feedback circuit to ELL pyramidal cells and are thought to be involved in a descending gain control mechanism that regulates the sensitivity of ELL pyramidal cells (Bastian 1986a,b). Bastian and Bratton (1990) compared the mean firing rates of NPd multipolar neurons at 30 and 240 s after experimentally induced step changes in global transdermal potential and noted a sustained change in firing rate over this time period that was roughly proportional to the transdermal voltage change. They concluded that NPd multipolar neurons have a tonic response component that reflects the mean amplitude of the transdermal potential.

The tonic response of NPd multipolar neurons presumably originates with P-type afferent input, which is relayed to NPd multipolar cells via the ELL. However, our analysis of the adaptation time course indicates that there probably is not a true tonic component to P-type afferent responses, raising the question of what role P-type afferents play in the apparent tonic responses observed in NPd multipolar neurons. Using a value of $B = 0.15$ in *Eq. 1*, we calculate that the mean afferent firing rate is expected to decline by ~17% over the time interval from 30 to 240 s. If reflected as a comparable change in NPd multipolar neuron firing rate, this modest change over a period of several minutes might have been unresolved by Bastian and Bratton (1990). If, on the other hand, NPd responses actually are more tonic than the afferents, there are at least two possible explanations. First, there may exist a subset of P-type afferents that have a more tonic response component, but which were not included in our sample. Because we only recorded from the posterior branch of the anterior lateral line nerve (ALLN), which innervates trunk electroreceptors, we cannot rule out the existence of a subclass of P-type afferents with more tonic response characteristics in the head region of the fish, which is innervated by other branches of the ALLN. A second possibility is that some sort of central integration mechanism extends the time course of NPd multipolar neuron responses relative to primary afferents. Such a neural integrator appears to be involved in the mammalian vestibulo-ocular reflex (VOR), for example, in which the dominant time constant of the overall reflex is typically several times longer than that of the vestibular afferents that drive it (Robinson 1981). In the VOR literature, this phenomenon is referred to as velocity storage. It is conceivable that the

electrosensory system could employ a similar mechanism for transdermal potential storage, which would enable certain central neurons to retain information about the global level of the transdermal potential for time periods that outlast the signals conveyed directly by primary electrosensory afferents.

REFERENCES

BASTIAN, J. Electrosensory input to the corpus cerebelli of the high frequency electric fish *Eigenmannia virescens*. *J. Comp. Physiol.* 90: 1–24, 1974.

BASTIAN, J. Electrolocation. I. How the electroreceptors of *Apteronotus albifrons* code for moving objects and other electrical stimuli. *J. Comp. Physiol.* 144: 465–479, 1981a.

BASTIAN, J. Electrolocation. II. The effects of moving objects and other electrical stimuli on the activities of two categories of posterior lateral line lobe cells in *Apteronotus albifrons*. *J. Comp. Physiol.* 144: 481–494, 1981b.

BASTIAN, J. Gain control in the electrosensory system mediated by descending inputs to the electrosensory lateral line lobe. *J. Neurosci.* 6: 553–562, 1986a.

BASTIAN, J. Gain control in the electrosensory system: a role for the descending projections to the electrosensory lateral line lobe. *J. Comp. Physiol.* 158: 505–515, 1986b.

BASTIAN, J. AND BRATTON, B. Descending control of electroreception. I. Properties of nucleus praeeminentialis neurons projecting indirectly to the electrosensory lateral line lobe. *J. Neurosci.* 10: 1226–1240, 1990.

BASTIAN, J. AND COURTRIGHT, J. Morphological correlates of pyramidal cell adaptation rate in the electrosensory lateral line lobe of weakly electric fish. *J. Comp. Physiol. A* 168: 393–407, 1991.

BASTIAN, J. Electrosensory organisms. *Physics Today* 47: 30–37, 1994.

BENNETT, M. V. L., SANDRI, C., AND AKERT, K. Fine structure of the tuberous electroreceptor of the high-frequency electric fish, *Sternarchus albifrons* (gymnotiformes). *J. Neurocytol.* 18: 265–283, 1989.

BRATTON, B. AND BASTIAN, J. Descending control of electroreception. II. Properties of nucleus praeeminentialis neurons projecting directly to the electrosensory lateral line lobe. *J. Neurosci.* 10: 1241–1253, 1990.

BRETSCHNEIDER, F., DEWEILLE J. R., AND KLIS, J. F. K. Functioning of catfish electroreceptors: fractional-order filtering and non-linearity. *Comp. Biochem. Physiol. A* 80: 191–198, 1985.

BULLOCK, T. H. AND HEILIGENBERG, W. *Electroreception*. New York: John Wiley and Sons, 1986.

FRENCH, A. S. AND TORKKELI, P. H. The time course of sensory adaptation in the cockroach tactile spine. *Neurosci. Lett.* 178: 147–150, 1994.

HAGIWARA, S., SZABO, T.. AND ENGER, P. S. Electroreceptor mechanisms in a high-frequency weakly electric fish, *Sternarchus albifrons*. *J. Neurophysiol.* 28: 784–799, 1965.

HEILIGENBERG, W. *Neural Nets in Electric Fish*. Cambridge: MIT Press, 1991.

HOPKINS, C. D. Stimulus filtering and electroreception: tuberous electroreceptors in three species of gymnotid fish. *J. Comp. Physiol.* 111: 171–207, 1976.

KNUDSEN, E. I. Spatial aspects of the electric field generated by weakly electric fish. *J. Comp. Physiol.* 99, 103–118, 1975.

MONTGOMERY, J. C., COOMBS, S., CONLEY, R. A., AND BODZNICK, D. Hindbrain sensory processing in lateral line, electrosensory and auditory systems: a comparative overview of anatomical and functional similarities. *Auditory Neurosci.* 1: 207–231, 1995.

MOUNTAIN, D. C. AND HUBBARD, A. E. Computational analysis of hair cell and auditory nerve processes. In: *The Springer Handbook of Auditory Research: Auditory Computation*, edited by H. L. Hawkins, T. A. McMullen, A. H. Popper, and R. R. Fay. New York: Springer-Verlag, 1996, p. 121–156.

NELSON, M. E. Progress and potential for modeling the ELL. *J. Comp. Physiol. A* 173: 686–687, 1993.

NELSON, M. E. A mechanism for neuronal gain control by descending pathways. *Neural Comput.* 6, 242–254, 1994a.

NELSON, M. E. Adaptive filtering in the electrosensory system. In: *Computation in Neurons and Neural Systems*, edited by F. H. Eeckman. Boston: Kluwer, 1994b, p. 209–214.

NORWICH, K. H. AND MCCONVILLE, K. M. V. An informational approach to sensory adaptation. *J. Comp. Physiol. A* 168: 151–157, 1991.

PAYNE, J. R., XU, Z., AND NELSON, M. E. A network model of automatic gain control in the electrosensory system. In: *Computation in Neurons and Neural Systems*, edited by F. H. Eeckman. Boston: Kluwer, 1994, p. 203–208.

RASNOW, B., ASSAD, C., AND BOWER, J. M. Phase and amplitude maps of the electric organ discharge of the weakly electric fish, *Apteronotus leptorhynchus*. *J. Comp. Physiol. A* 172: 481–491, 1993.

ROBINSON, D. A. The use of control systems analysis in the neurophysiology of eye movements. *Annu. Rev. Neurosci.* 4: 463–503, 1981.

RUGGERO, M. A. Physiology and coding of sound in the auditory nerve. In: *The Springer Handbook of Auditory Research. The Mammalian Auditory Pathway: Neurophysiology*, edited by A. N. Popper and R. R. Fay. New York: Springer-Verlag, 1992, vol. 2, p. 34–93.

SCHEICH, H., BULLOCK, T. H., AND HAMSTRA, R. H. Coding properties of two classes of afferent nerve fibers: high frequency electroreceptors in the electric fish, *Eigenmannia*. *J. Neurophysiol.* 36: 39–60, 1973.

SHUMWAY, C. A. Multiple electrosensory maps in the medulla of weakly electric gymnotiform fish. I. Physiological differences. *J. Neurosci.* 9, 4388–4399, 1989.

SHUMWAY, C. A. AND MALER, L. GABAergic inhibition shapes temporal and spatial response properties of pyramidal cells in the electrosensory lateral line lobe of gymnotiform fish. *J. Comp. Physiol. A* 164: 391–407, 1989.

SZABO, T. Anatomy of the specialized lateral line organs of electroreception. In: *Handbook of Sensory Physiology*, edited by A. Fessard. Berlin: Springer-Verlag, 1974, vol. 3, p. 13–58.

THORSON, J. AND BIEDERMAN-THORSON, M. Distributed relaxation processes in sensory adaptation. *Science Wash. DC* 183: 161–172, 1974.

XU, Z., PAYNE, J. R., AND NELSON, M. E. System identification and modeling of primary electrosensory afferent response dynamics. In: *Computation in Neurons and Neural Systems*, edited by F. H. Eeckman. Boston: Kluwer Academic Publishers, 1994, p. 197–202.

ZAKON, H. H. The electroreceptive periphery. In: *Electroreception*, edited by T. H. Bullock and W. Heiligenberg, New York: John Wiley and Sons, 1986, p. 103–156.

ZAKON, H. H. Differentiation and functional organization of tuberous receptors in *Sternopygus*. *J. Comp. Physiol. A* 173: 713–715, 1993.